Continuum model of mechanical interactions between biological cells and artificial nanostructures

Piyush Verma, Ian Y. Wong, and Nicholas A. Melosh[a)]
Department of Materials Science and Engineering, Geballe Laboratory for Advanced Materials, Stanford University, Stanford, California 94305

(Received 8 March 2010; accepted 29 April 2010; published 21 May 2010)

The controlled insertion of artificial nanostructures into biological cells has been utilized for patch clamping, targeted drug delivery, cell lysing, and cell mechanics measurements. In this work, an elastic continuum model is implemented to treat the deformation of spherical cells in solution due to their interaction with cylindrical probes. At small deformations, the force varies nonlinearly with indentation due to global deformation of the cell shape. However, at large indentations, the force varies linearly with indentation due to more localized deformations. These trends are consistent with experimental measurements under comparable conditions and can be used to develop design rules for optimizing probe-cell interactions. © *2010 American Vacuum Society.*
[DOI: 10.1116/1.3431960]

I. INTRODUCTION

Engineering the mechanical interactions between artificial nanostructures and cell membranes represents a powerful approach for understanding and regulating biological systems. For example, sharpened structures such as glass pipettes or AFM tips have been used to characterize mechanical properties of biological cells.[1–3] The insertion of inorganic nanowires or carbon nanotubes through these membranes can also allow electrical and biochemical access into the cell interior.[4–9] The cellular uptake of micro- and nanoparticles through alternate pathways such as endocytosis or phagocytosis[10] have been explored for targeted drug delivery or gene therapy.[11–15] Finally, the use of topographical patterning at the nanoscale can have dramatic effects on cellular phenotype and organization.[16,17]

These interactions are dependent on the viscoelastic properties of cellular membranes, which have been characterized through a variety of techniques, including micropipette aspiration, atomic force microscopy, microchannel flow, and optical tweezers.[18] Quantitative measurements of membrane tension and compression modulus have been utilized in both continuum and finite-element models of cell mechanics. Most of the models for cellular deformation are continuum models based on micropipette aspiration, which model the process either as the deformation of a viscoelastic solid cell body (solid models)[19,20] or as the flow of a fluid inside a membrane (fluid models).[21–23] Although these models have been very successful in elucidating the pipette-cell system, their broader applicability is limited due to the use of parameters and boundary conditions highly specific to these experimental scenarios, as well as their mathematical complexity. The other class of cellular deformation models is that of phenomenological models such as the sol-gel model, soft glassy rheology, or tensegrity.[24] These models seek to explain the unusual rheological properties of biological cells and how they might arise from the molecular interactions of cytoskeletal polymers and motor proteins. However, they have not yet been applied to detailed cell shape calculations, particularly for free cells.

Here, we present an elastic continuum model that treats the large-scale deformation of an unattached spherical cell interacting with a cylindrical probe (Fig. 1). This geometry is relevant for lab-on-a-chip platforms that use microfabricated pillars or nanoscale electrodes on flat surfaces, as well as transfection of nonadherent cells using microinjection. Since the focus of this work is on the large-scale deformation of membranes, it does not account for any local stress concentration that might arise due to interaction with very sharp probes. However, an increased understanding of the interactions between cell membranes and probe surfaces is essential for the development of membrane-fusing "stealth" nanostructures with heterogeneously functionalized sidewalls.[25]

The cell is treated as a nonadherent elastic body which deforms on contact with the cylindrical probe. This is a crucial distinction from the scenario considered by Sen *et al.*,[26] where the cell is strongly fixed on a substrate and contacted by an external probe from solution, modeled by holding the cell footprint constant. The different boundary conditions imposed here drive a dramatically different evolution of cell shape profile with probe indentation. Initially, the cell exhibits its global shape deformation at small indentations but transitions to a more localized deformation at larger indentations. This trend corresponds to a nonlinear to linear scaling of indentation force with indentation distance that has been previously observed experimentally in an analogous system of polymeric vesicles.[27] These effects have a strong dependence on probe diameter, which suggests design rules for optimizing the interactions between biological cells in solution and nanofabricated structures on a surface for lab-on-a-chip applications. Moreover, this model may yield novel insights into the mechanical behavior of cells that are not strongly adherent to a surface.

a)Electronic mail: nmelosh@stanford.edu

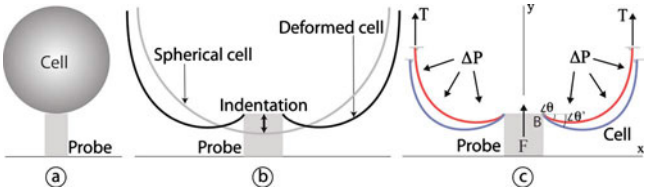

FIG. 1. (a) (Color online) Nonadherent cell in solution in contact with a probe fabricated on a substrate. (b) Schematic showing the snapshot of the original cell and the deformed cell, offset to keep the center of the cell fixed. (c) Free body diagram of the half cell. F, ΔP, and T represent the indentation force, the pressure difference, and the membrane tension, respectively. Note how the cell flattens and expands laterally to conserve the total volume.

II. THEORY

The scenario of a nonadherent cell in solution interacting with a cylindrical probe [Fig. 1(a)] is treated through the following theoretical framework. The cell is assumed to be initially spherical with a radius R_c=4 μm, which is comparable to the size of a red blood cell. It is axisymmetrically indented by a cylindrical probe whose diameter is varied from 1 μm down to 10 nm, to treat a range of possible probe types from microelectrodes down to inorganic nanowires. Under these conditions, gravitational forces are relatively weak (approximately piconewtons). Instead, the probe-cell interactions may arise from externally applied forces such as micropipette manipulation or fluid flow. The cell is assumed to be incompressible, so that its volume is conserved at the cost of increasing surface area with deformation. This energetic cost of area expansion arises from the cell membrane, which consists of various proteins and carbohydrates embedded in a fluid lipid bilayer. The cell membrane is approximated by an average isotropic elastic sheet with a characteristic bending rigidity and area expansion modulus. Since the membrane is very thin, the effect of bending energy on membrane tension is neglected.[28] The shear deformation energy is also assumed to be negligible compared to the dilational energy contribution.[29] Under these conditions, the membrane tension can be assumed to be uniform throughout the surface of the membrane.[30] The deformation of the membrane due to the force applied by a cylindrical probe is given (to leading order) by the Young–Laplace equation:[31]

$$\frac{1}{R_m}+\frac{1}{R_\phi}=\frac{\Delta P}{T}=\text{const}, \tag{1}$$

where T is the isotropic tension in the membrane, ΔP is the hydrostatic pressure, and R_m and R_ϕ are the principal curvatures of the membrane. Experimentally, the deformed contour of preswollen red blood cells has been shown to follow this condition, wherein the mean curvature is constant at every point on the membrane.[32]

By incorporating a gradually varying boundary condition at the probe surface and utilizing the Young–Laplace equation under the constraint of constant volume, the cell shape profile can be successively calculated at varying probe insertions (indentations) to a depth h. In particular, as the cell is deformed due to indentation by the probe, the contact angle at point B [Fig. 1(c)] is assumed to vary smoothly from 0° to 90°. Once the contact angle at point B reaches 90°, the membrane begins to conform with the sidewalls of the probe. In this regime, the contact angle of the membrane with the probe stays constant at 90°; however, it keeps deforming to maintain a fixed volume at increasing indentations.

As the cell deforms and its surface area increases with indentation, the membrane tension is assumed to increase linearly with the fractional increase in area.[33–35] The indentation force F of the probe can be determined from a force balance with terms corresponding to hydrostatic pressure and membrane tension, as shown in Fig. 1(c):

$$F=\Delta P(\pi R_2^2)-(T_0+K_a\alpha)2\pi R_2, \tag{2}$$

where R_2 is the equatorial radius of the cell that varies with membrane deformation, T_0 is the membrane tension at zero deformation, K_a is the elastic expansion modulus for area deformation, and α is the fractional area expansion. In this scheme, the primary contribution to membrane deformation is assumed to arise from this mechanism. Although this is appropriate for the probe diameters considered here, probes with sharp geometries generate local stresses that may nucleate membrane rupture. This scenario will be considered elsewhere.

This theoretical framework of a mobile, unattached spherical cell interacting with a cylindrical probe structure [Fig. 1(a)] is analogous to the case of axisymmetric loading of a thin spherical shell using the equations of membrane elasticity. This scenario is particularly difficult to treat analytically due to the nonlinearities inherent in this geometric configuration.[36] Instead, the numerical solution implemented here offers a convenient and accurate solution where the convergence of the analytical solution is slow.

III. RESULTS AND DISCUSSION

Figure 2 shows the evolution of the cell shape profile at successive indentation for the representative cases of 1 μm and 100 nm diameter probes. In both cases, the assumption of volume conservation causes the cell to both flatten vertically and swell laterally with increasing indentation. The extent of this swelling depends strongly on the probe diameter d_P since the cell is more strongly distorted by the displaced volume of larger probes. For example, for a large probe with d_P=1 μm, the cell swells laterally by approximately 150 nm over the course of the 1.3 μm indentation in profiles A–C. In comparison, for a much smaller probe with d_P=100 nm, the cell swells laterally by only 15 nm for the same indentation in profiles U–Y.

A closer examination of successive cell shape profiles near the probe [Figs. 2(b) and 2(d)] reveals a surprising trend. Initially, for small indentations, the cell shape undergoes a global shape deformation (A→C or U→W). However, beyond a critical indentation h', the cell shape deformation becomes much more localized to the proximity of the probe (C→E or W→Z). These deformations can be quantified by comparing successive cell shape profiles, correcting for the vertical displacement of the cell through an offset

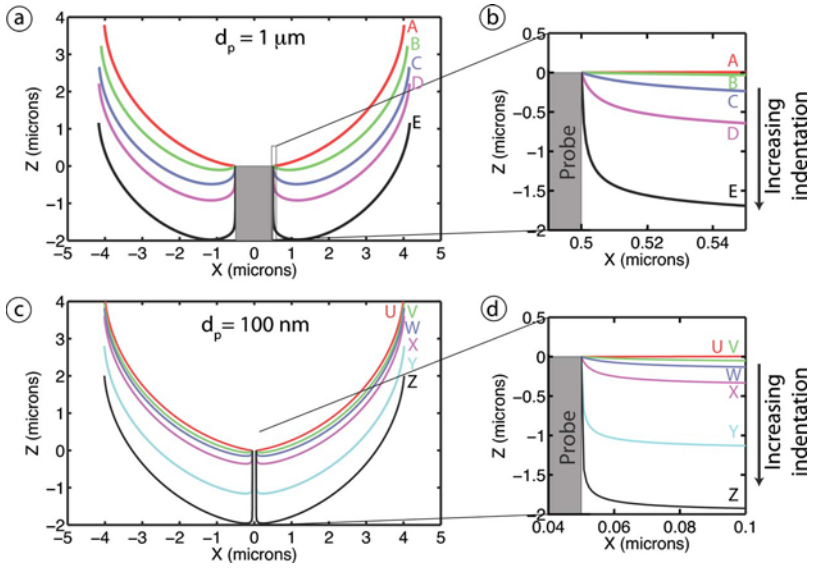

FIG. 2. (Color online) Successive shape profiles of the cell with increasing deformation as it is indented by the probe. The probe is assumed to be 2 μm in height. (a) Deformation against a thick probe 1 μm in diameter. A–E refer to intermediate deformation profiles of the cell. (b) Deformation profiles close to the 1 μm diameter probe. (c) Deformation against a thin probe 100 nm in diameter. U–Z refer to intermediate deformation profiles of the cell. (d) Deformation profiles close to the 100 nm diameter probe. The thin 100 nm probe is in much more conformal contact with the cell membrane as compared to the thick 1 μm probe.

proportional to the indentation so that the center of the cell does not change (Fig. 3). The difference in successive cell shape profiles Δy is shown in Fig. 4 for the representative cases of d_P=1 μm and d_P=100 nm. For the former case, during the transition from A→B as well as B→C, Δy is nonzero for all values of x, which represents global changes in cell shape for small indentation [Fig. 4(a)]. Δy changes sign at intermediate values of x, which corresponds to the intersection of the cell shape profiles and is an artifact due to the applied offset (Fig. 3). In the limit of large indentations like for C→D or D→E, Δy is zero everywhere but near the immediate vicinity of the probe [Fig. 4(c)]. Thus, the shape change in this regime is highly localized near the probe with minimal global distortion. The case for indentation by a probe with d_P=100 nm shows similar trends in deformation as the shape change transitions from being global at small indentations [Fig. 4(b)] to being localized around the probe for large indentation [Fig. 4(d)].

A useful metric for quantifying this deformation can be defined in terms of the lateral position of the minimum point on the cell shape profile (Fig. 5). For small indentations, the global deformation of the cell is exhibited by a large lateral shift in $x_{\min}$ of ~0.6 μm from A→B and ~0.2 μm from U→X, for d_P=1 μm and 100 nm, respectively [Fig. 5(c)]. At larger indentations, the cell membrane becomes nearly conformal with the probe surface, resulting in more localized deformation that leaves the global cell shape profile largely unchanged. Thus, there is negligible change of 10–15 nm in $x_{\min}$ in the limit of large deformations from C→D and X→Y, for d_P=1 μm and 100 nm, respectively. These curves can be rescaled to comparable values by nondimensionalizing the indentation by the geometric mean of probe radius and cell radius, i.e., $h^*=2h/\sqrt{r_P R_C}$ and $x_{\min}$ by cell radius, $x_{\min}{}^*=x_{\min}/R_C$ [Fig. 5(d)].

Since volume is conserved, the large lateral deformations observed for small indentations correspond to small vertical deformations. Conversely, the small lateral deformations observed at large indentations correspond to larger vertical deformations. This is quantified through the vertical position of the minimum point $y_{\min}$ on the cell shape profile [Figs. 5(e) and 5(f)]. For small indentations (A→B or U→X), there are vertical shifts of $y_{\min}$=0.1 and 0.3 μm, respectively, for 1 μm and 100 nm diameter probes. In the limit of larger indentations (B→C or X→Y), there are larger vertical shifts of $y_{\min}$=0.4 μm and 0.8 μm, respectively, for 1 μm and 100 nm diameter probes. The overall variation in $y_{\min}$ as a function of indentation h is shown in Fig. 5(e). As the probe diameter increases from 10 nm to 1 μm, the transition from global deformation to local deformation occurs at larger and

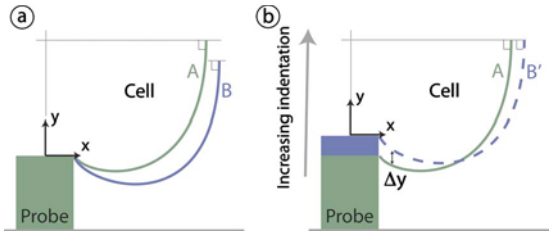

FIG. 3. (Color online) (a) Schematic of two snapshots of the deformed cell profiles at successive indentation. (b) Shape profile B offset to keep the center of the cell fixed. Variation in Δy along x shows where the shape change occurs.

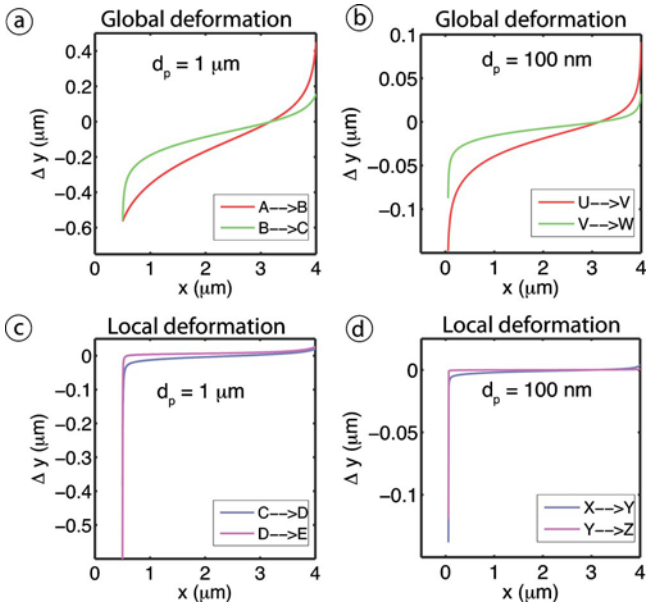

FIG. 4. (Color online) Differences in subsequent cell deformation profiles Δy near the probe surface. The deformation profiles selected are the same as the ones marked in Fig. 2. (a) Small indentations with $d_p=1$ μm. A$\rightarrow$B corresponds to the subtraction of cell profile B (adjusted for height) from cell profile A, etc. Large Δy at all values of x indicates a global change in the shape of the cell. (b) Small indentations with $d_p=100$ nm show global deformations in cell shape that are similar to (a). (c) Large indentations with $d_p=1$ μm. A large Δy only at x close to the probe surface and zero everywhere else indicates a local change in the shape of the cell. (d) Large indentations with $d_p=100$ nm show local deformations in cell shape that are similar to (c).

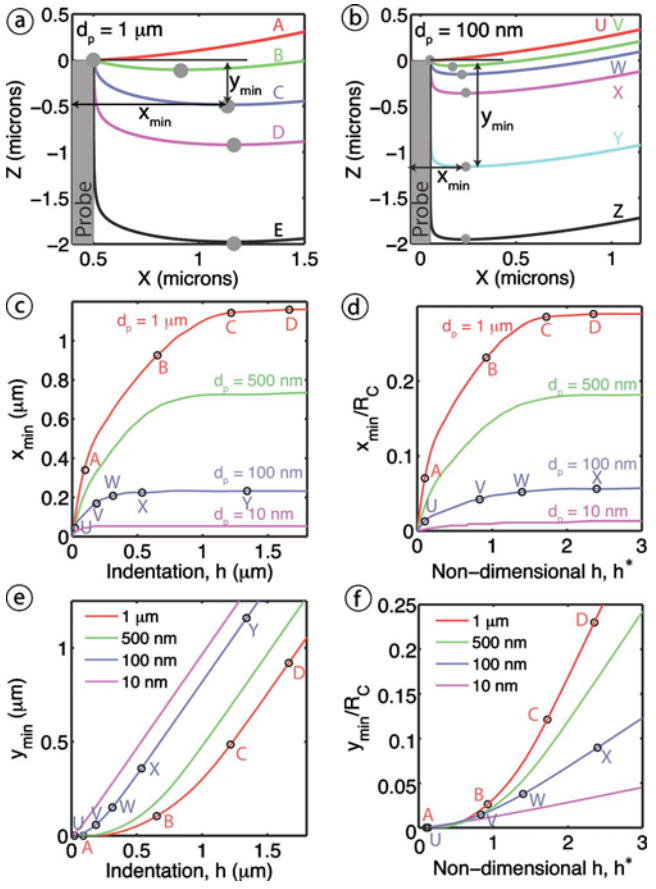

FIG. 5. (Color online) Cell shape profiles near the probe, (a) for a probe 1 μm in diameter, and (b) for a probe 100 nm in diameter. Letters A, B, C,…,U, V, W,… are the cell shape profiles at specific indentations, same as in Fig. 2. The point on the cell membrane closest to the substrate is indicated on all profiles by a gray circle; it has coordinates $(x_{\min},y_{\min})$. (c) Variation of $x_{\min}$ with indentation for different probe sizes. $x_{\min}$ plateaus at the nonlinear to linear transition. (d) $x_{\min}$ normalized with cell radius, plotted against dimensionless indentation, $h^*=2h/\sqrt{r_p}\sqrt{R_C}$. The dimensionless indentation at transition, marked by the onset of the plateau region, collapses to order unity for different probe sizes. (e) Variation of $y_{\min}$ with indentation for different probe sizes. Note the nonlinear to linear transition. (f) Variation of $y_{\min}$ normalized by the cell radius with dimensionless indentation, h^*. Similar to (d), the indentation at transition collapses to order unity.

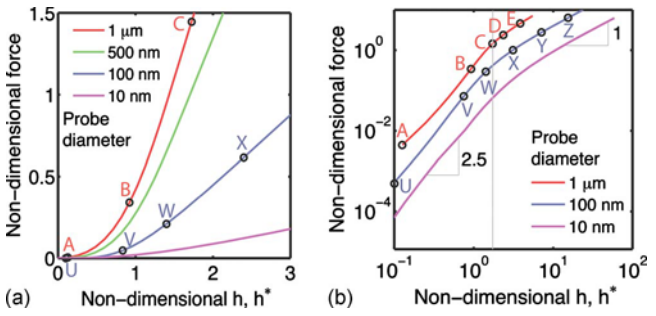

FIG. 6. (Color online) Effect of probe diameter on the vertical force exerted by the cell on the probe as a function of indentation. The force is nondimensionalized with the product of maximum membrane tension and probe radius. (a) Force-indentation curves on a linear scale; note the nonlinear to linear transition similar to Figs. 5(e) and 5(f). (b) Force-indentation curves on a log-log scale. The nonlinear region has a slope of about 2.5. The nonlinear to linear transition occurs at a nondimensional indentation of order unity.

larger critical indentations h'. Beyond this critical indentation, the lateral minimum position $x_{\min}$ approaches a plateau value, whereas the vertical minimum position $y_{\min}$ increases rapidly.

The critical transition from global deformation regime and local deformation regime can be more easily compared by rescaling the indentation with the geometric mean of probe diameter and cell radius, i.e., $h^*=2h/\sqrt{r_pR_C}$. The horizontal and vertical coordinates of the minimum of the cell shape profile are similarly rescaled by the cell radius, i.e., $x_{\min}{}^*=x_{\min}/R_C$ and $y_{\min}{}^*=y_{\min}/R_C$. After this rescaling, the critical transition now occurs when the indentation is order unity, $h^*\sim 1$, for all probe diameters [Figs. 5(d) and 5(f)]. This critical value delineates a transition between a highly nonlinear regime at small indentations and a linear regime at larger indentations. Intriguingly, a comparable transition occurs when comparing the indentation force F_{indent} and indentation displacement h for all probe diameters (Fig. 6). As the probe diameter increases from 10 nm to 1 μm, the necessary force F to reach a given indentation h increases since the cell must undergo more distortion to conform to the probe. These can be compared in a similar manner by rescaling force with the product of maximum membrane tension and probe radius. Such a transition has been observed experimentally in a comparable but nonbiological system when polymeric vesicles freely suspended in solution were indented with flat tipped microcantilevers.[27] For the case of indentation of

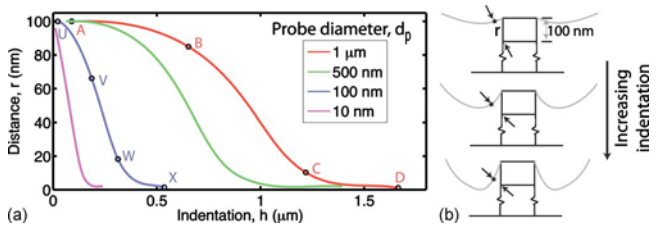

FIG. 7. (Color online) (a) Proximity of the cell membrane to a fixed location on the probe as the cell is indented by probes with different diameters, measured as the shortest distance r between this location and cell membrane. The fixed location is arbitrarily defined to be 100 nm away from the top of the probe. r increases with increasing probe diameter due to the difficulty of deforming around large probes. (b) Schematic showing how this distance r changes with indentation.

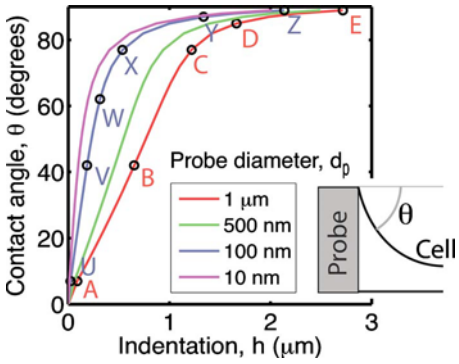

FIG. 8. (Color online) Change in the contact angle, θ, of the cell membrane at the probe tip with indentation, shown here for different probe diameters. The contact angle at the probe is less than 90° at the transition point (C or W), indicating that the transition does not correspond to conformal contact with the probe.

these polymeric vesicles by sharp cantilevers, only the linear regime was observed experimentally as the measured indentations are much larger compared to the critical indentation. However, this transition is the exact opposite of what was observed (a linear to nonlinear transition) by Sen *et al.* for cells that are strongly adherent to a substrate. These dramatically different trends arise from the different boundary conditions implemented in the respective models.

The nonlinear to linear transition becomes more apparent when the data are replotted on a log-log scale [Fig. 6(b)]. Over the 2 decades in probe diameter considered here, the force in the nonlinear small-indentation regime consistently scales as a power law in displacement with an exponent of 2.5 ± 0.1. However, in the linear large-indentation regime, the force is linear in displacement with an exponent of 1 ± 0.2.

$$F \propto (h^*)^{2.5} \quad \text{for small indentations},$$

$$F \propto (h^*)^{1.0} \quad \text{for large indentations}.$$

Given the nonlinearity inherent in this geometry, the physical origin of this particular scaling dependence remains unclear.[36] The scaling exponent of 2.5 observed in the nonlinear regime is close to the exponent of 2.66 found by Hategan *et al.* for the deformation of a spherical membrane by an attached spherical bead.[37,38]

In order to elucidate the origin of this transition from global to local deformation, the cell shape deformation near the surface is examined through two metrics. First, the proximity of the membrane to a fixed location on the probe surface is considered (Fig. 7). The minimum distance between this location and the cell membrane continually decreases with increasing indentation as the cell deforms around the probe. One possibility is that the global to local transition occurs when the cell comes into conformal contact with the probe at sufficiently large indentations, h_C. However, the critical indentation h' appears to occur well before conformal contact. For example, at the transition points C and W for the $d_p = 1$ μm and 100 nm, respectively, the membrane is still found to be at a minimum distance of 15 and 20 nm, respectively, from the fixed location on the probe. Conformal contact does not occur until well into the nonlinear regime, i.e., beyond points X and D, respectively. Moreover, the indentation at which the cell conformally contacts the probe at this point increases from about $h_C = 1$ μm for $d_P = 100$ nm to $h_C = 2$ μm for $d_P = 1$ μm, due to the difficulty of deforming around large probes. This trend is corroborated by the use of a second metric, the contact angle of the membrane with the top of the probe (Fig. 8). The contact angle at the critical transition h', which corresponds to point C for the 1 μm probe case, is found to be about 75°. In contrast, the cell membrane conformally contacts the probe surface for contact angles of 90° or greater. Similarly, for the 100 nm diameter probe, the contact angle at the critical indentation h^* occurs at point W, which corresponds to a contact angle of slightly over 60°.

It should be noted that cells can be lysed at sufficiently large indentations due to excessively large area strains. This is an important consideration when optimizing nanostructure geometries for lab-on-a-chip applications. For example, promoting cell lysis may be preferable for extracting cell contents for subsequent molecular analysis.[39] However, applications such as patch clamping or drug delivery would be more effective if good conformal contact can be achieved without lysing. The maximum safe area strain corresponding to the onset of lysing can be estimated by $\alpha = 3 \pm 0.7\%$ based on experimental measurements on red blood cells by Evans *et al.*[40] This can be compared to the increase in membrane surface area and effective tension computed from the change in cell shape profiles at increasing indentations (Fig. 9). As probe diameter increases, this maximum allowable indentation decreases since the cell undergoes much larger deformation to accommodate the increased probe volume. For instance, with probes of $d_p = 1$ μm or 500 nm, this unsafe area strain corresponds to maximum allowable indentations of 1.3 and 2.2 μm, respectively. This is comparable to experimental observations for transfection using microinjectors, where 1 μm insertion is sufficient to introduce genetic material inside the cell. However, for smaller probes of 100 or 10 nm in diameter,[41,42] lysing will not occur due to area strain mechanisms even for very large indentations. Instead, at these molecular length scales, lysing may occur due to other

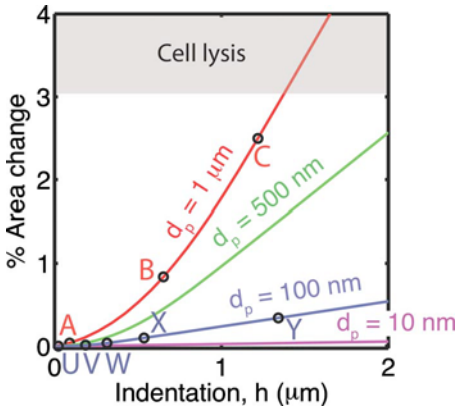

FIG. 9. (Color online) Percentage change in area of the cell membrane with indentation for different probe sizes. The region marked cell lysis is where the membrane area strain is greater than 3%.

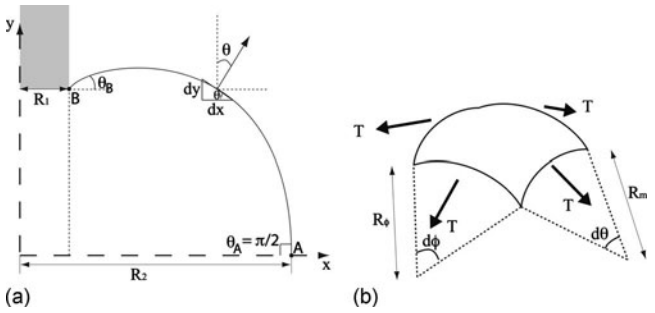

FIG. 10. (a) Geometry and notation used to calculate the cell shape. The probe, which has a radius R_1, is shown in gray. The boundary conditions for the shape are specified in terms of the contact angles θ_A and θ_B at distances R_2 and R_1 from the y-axis, respectively (b) Free body diagram of a membrane patch showing the direction of membrane tension. The meridional and circumferential radii of curvature are also shown.

physical mechanisms such as pore nucleation and growth due to local stress hotspots. These mechanisms have not been addressed here but will be explored in future work.

One assumption of this model is that the membrane tension increases linearly with fractional change in area. Although this assumption is appropriate for swollen blood cells, it may not hold for other types of eukaryotic cells, which possess different membrane structures and viscoelastic properties. These could include large membrane reserves (i.e., membrane folds or protrusions) or nonlinear elasticities. Nevertheless, this scheme can be easily adapted to address those considerations by varying the dependence of tension with area dilation.

Another important assumption is that mechanical deformation occurs under equilibrium conditions. This holds for red blood cells, but most eukaryotic cells exhibit coordinated, nonequilibrium structural rearrangements. These active mechanisms may play a role in recent experiments where cells impale themselves on arrays of nanowires.[9] In these experiments, the cell-substrate adhesions could generate additional downward forces for indentation, but this has not been established. Even so, the theoretical model developed here is expected to be relevant for two general scenarios. First, equilibrium deformation should be appropriate for fast timescales where the cell does not have sufficient time to respond. Second, this model is likely to be the limiting case for larger probes where the volume becomes comparable to the cell size, since it is extremely difficult for large-scale nonequilibrium rearrangements to occur.

IV. CONCLUSIONS

The deformation of spherical cells in solution due to the axisymmetric indentation by a cylindrical probe is treated using an elastic continuum model. Consistent with previous experimental measurements in this geometry, the indentation force exhibits a nonlinear to linear transition with increasing indentation. This can be explained phenomenologically in terms of a global cell deformation regime at small indentations which transitions to more localized deformations at larger indentations. As probe diameter increases, this critical transition occurs at larger indentations, since the cell undergoes larger deformations to accommodate the volume of larger probes. However, it appears that this critical transition is not due to the onset of conformal contact between the probe surface and cell membrane.

This model reveals certain nontrivial trends in cell deformation and membrane tension due to probe-cell interactions that are relevant for lab-on-a-chip design, cell transfection, and mechanobiology. First, it can be used to estimate the minimum indentation distance necessary to achieve conformal contact of the cell membrane with the probe, allowing biochemical or electrical access to the cell interior. In addition, it can be used to estimate the maximum indentation distance where cells do not get lysed due to excessive area strain. Finally, the transition from nonlinear to linear regimes in indentation represents a limiting case for cells that are not adherent to a surface. This may yield qualitative insight for experimental scenarios where cells are only weakly adherent, including surfaces that are topographically patterned on the micro- or nanoscale.

ACKNOWLEDGMENTS

The authors thank T.-f. Wong for helpful discussions. P.V. was funded by the Stanford Center for Integrated Systems. I.Y.W. was funded by the NSF Grant No. CBET-0827822.

APPENDIX

Figure 10 shows the notation used in the following analysis. If T is the isotropic tension in the membrane, ΔP is the hydrostatic pressure, and R_m and R_ϕ are the principal curvatures of the membrane, applying a force balance on a patch of membrane, as shown in Fig. 10(a), gives

$$\frac{1}{R_m} + \frac{1}{R_\phi} = \frac{\Delta P}{T} = \text{const.} \tag{A1}$$

Using the Frenet–Serret relation, this equation becomes

$$\frac{du}{dx}+\frac{u}{x}=\text{const} \quad \text{where} \quad u=\sin\theta, \tag{A2}$$

with boundary conditions—$x=R_1$, $\theta=-\theta_B$ and $x=R_2$, $\theta=\theta_A=90°$. Angle θ_A is fixed at 90° so that when the curve if reflected about the x-axis, it remains smooth. Thus, the shape of the entire cell can be computed by solving for the cell shape in just one quadrant.

The solution to the differential equation (A2) can be determined by multiplying it with an integrating factor $e^{\int(1/x)dx}$. The solution is

$$u=c_1x+\frac{c_2}{x}, \tag{A3}$$

where

$$c_1=\frac{R_1\sin\theta_B+R_2}{R_2^2-R_1^2} \quad \text{and} \quad c_2=\frac{R_1R_2(R_1+R_2\sin\theta_B)}{R_1^2-R_2^2}.$$

As the cell is deformed due to indentation by the probe, the contact angle at point B is assumed to vary smoothly from 0° to 90°. Once the contact angle at point B reaches 90°, the membrane begins to conform with the sidewalls of the probe. In this regime, the contact angle of the membrane with the probe stays constant at −90°; however, it keeps deforming to maintain a fixed volume at increasing indentations. For the nonconformal regime, the volume of quarter cell can be computed as the volume of the surface of revolution,

$$V=\int_{R_2}^{R_1}\pi x^2\frac{c_1x+\frac{c_2}{x}}{\sqrt{1-\left(c_1x+\frac{c_2}{x}\right)^2}}dx. \tag{A4}$$

For the regime where the membrane is in contact with the sidewalls of the probe, a volume equal to that of the cylinder swept by the probe was added to this computed volume. To solve the differential equation (A2) subject to the condition of constant volume, the following iterative scheme was used. The lateral swelling of the cell or the increase in R_2, ΔR_2 arbitrarily assigned an initial value. Using the solution (A3) to the differential equation, the volume of the cell was computed using expression (A4). A correction was applied to ΔR_2 in proportion to the difference between the initial volume of the spherical cell V_0 and the computed volume. This was done iteratively until the computed volume was equal to the initial volume V_0. From θ as a function of x, the y coordinate of the curve was determined using the following relation:

$$y=\int_{R_2}^{x}\tan\theta dx=\int_{R_2}^{x}\frac{c_1x+\frac{c_2}{x}}{\sqrt{1-\left(c_1x+\frac{c_2}{x}\right)^2}}dx. \tag{A5}$$

This calculation was repeated for different values of contact angle at point B in the range 0° to 90° to compute the entire shape evolution of the cell. From cell shape, indentation was computed as

$$h=R_0-\int_{R_2}^{R_1}\frac{c_1x+\frac{c_2}{x}}{\sqrt{1-\left(c_1x+\frac{c_2}{x}\right)^2}}dx, \tag{A6}$$

where R_0 is the radius of the undeformed spherical cell.

To calculate the membrane tension, the pressure difference, and the indentation force on the cell, consider the free body diagram of a cell sectioned at the midplane, as shown in Fig. 1(c). If f is the force exerted by the indentation probe,

$$T(2\pi R_2)+f=\Delta P(\pi R_2^2). \tag{A7}$$

The tension goes up linearly with the fractional area expansion, α, as[31]

$$T=T_0+K_a\alpha. \tag{A8}$$

For the purpose of these calculations, an area expansion modulus of $K_a=450$ mN/m^2 and zero initial tension corresponding to a free nonadherent cell are assumed.[40] To calculate this fractional area expansion, α, at any instant, the area expansion was computed using the initial area A_0 of the half cell as

$$\alpha=\frac{A-A_0}{A_0} \quad \text{where} \quad A=\int_{R_1}^{R_2}\frac{2\pi x}{\sqrt{1-\left(c_1x+\frac{c_2}{x}\right)^2}}dx. \tag{A9}$$

Thus, the indentation force can be calculated with deformation as

$$f=\Delta P(\pi R_2^2)-(T_0+K_a\alpha)2\pi R_2. \tag{A10}$$

From Eq. (1), we know that

$$\Delta P=\frac{1}{R_m}+\frac{1}{R_\phi}=2c_1T\Rightarrow f=2c_1T(\pi R_2^2)-T(2\pi R_2)\Rightarrow f$$
$$=(T_0+K_a\alpha)2\pi R_2(c_1R_2-1). \tag{A11}$$

[1] N. Hilal, W. Bowen, L. Alkhatib, and O. Ogunbiyi, Chem. Eng. Res. Des. **84**, 282 (2006).
[2] F. Gaboriaud and Y. F. Dufrene, Colloids Surf., B **54**, 10 (2007).
[3] Y. F. Dufrêne, Nat. Rev. Microbiol. **6**, 674 (2008).
[4] P. Sun, F. O. Laforge, T. P. Abeyweera, S. A. Rotenberg, J. Carpino, and M. V. Mirkin, Proc. Natl. Acad. Sci. U.S.A. **105**, 443 (2008).
[5] I. Kleps, M. Miu, F. Craciunoiu, and M. Simion, Proceedings of the 32nd International Conference on Micro- and Nano-Engineering [Microelectron. Eng. **84**, 1744 (2007)].
[6] W. Kim, J. K. Ng, M. E. Kunitake, B. R. Conklin, and P. Yang, J. Am. Chem. Soc. **129**, 7228 (2007).
[7] Y. Qiao, J. Chen, X. Guo, D. Cantrell, R. Ruoff, and J. Troy, Nanotechnology **16**, 1598 (2005).
[8] X. Chen, A. Kis, A. Zettl, and C. R. Bertozzi, Proc. Natl. Acad. Sci. U.S.A. **104**, 8218 (2007).
[9] A. K. Shalek *et al.*, Proc. Natl. Acad. Sci. U.S.A. **107**, 1870 (2010).
[10] S. D. Conner and S. L. Schmid, Nature (London) **422**, 37 (2003).
[11] M. E. Davis, Z. G. Chen, and D. M. Shin, Nat. Rev. Drug Discovery **7**, 771 (2008).
[12] W. Jiang, B. Y. S. Kim, J. T. Rutka, and W. C. W. Chan, Nat. Nanotechnol. **3**, 145 (2008).
[13] B. D. Chithrani, A. A. Ghazani, and W. C. W. Chan, Nano Lett. **6**, 662 (2006).

[14]J. A. Champion and S. Mitragotri, Proc. Natl. Acad. Sci. U.S.A. **103**, 4930 (2006).
[15]S. Mitragotri and J. Lahann, Nature Mater. **8**, 15 (2009).
[16]R. G. Thakar, M. G. Chown, A. Patel, L. Peng, S. Kumar, and T. A. Desai, Small **4**, 1416 (2008).
[17]M. M. Stevens and J. H. George, Science **310**, 1135 (2005).
[18]T. Brown, J. Biomech. **33**, 3 (2000).
[19]G. W. Schmidschonbein, K. L. Sung, H. Tozeren, R. Skalak, and S. Chien, Biophys. J. **36**, 243 (1981).
[20]D. P. Theret, M. J. Levesque, M. Sato, R. M. Nerem, and L. T. Wheeler, J. Biomech. Eng. **110**, 190 (1988).
[21]E. Evans and A. Yeung, Biophys. J. **56**, 151 (1989).
[22]D. Needham and R. M. Hochmuth, J. Biomech. Eng. **112**, 269 (1990).
[23]C. Dong, R. Skalak, and K. L. Sung, Biorheology **28**, 557 (1991).
[24]B. D. Hoffman and J. C. Crocker, Annu. Rev. Biomed. Eng. **11**, 259 (2009).
[25]B. D. Almquist and N. A. Melosh, Proc. Natl. Acad. Sci. U.S.A. **107**, 5815 (2010).
[26]S. Sen, S. Subramanian, and D. E. Discher, Biophys. J. **89**, 3203 (2005).
[27]V. Gordon, C. Xi, J. Hutchinson, A. Bausch, M. Marquez, and D. Weitz, J. Am. Chem. Soc. **126**, 14117 (2004).
[28]B. Daily, E. L. Elson, and G. I. Zahalak, Biophys. J. **45**, 671 (1984).
[29]E. A. Evans and R. Skalak, CRC Crit. Rev. Bioeng. **3**, 181 (1979).
[30]R. Aris, *Vectors, Tensors, and the Basic Equations of Fluid Mechanics* (Prentice-Hall, Englewood Cliffs, NJ, 1962).
[31]D. H. Boal, *Mechanics of the Cell* (Cambridge University Press, Cambridge, UK, 2002).
[32]E. A. Evans, Biophys. J. **30**, 265 (1980).
[33]E. Evans and W. Rawicz, Phys. Rev. Lett. **64**, 2094 (1990).
[34]B. M. Discher, Y. Y. Won, D. S. Ege, J. C. Lee, F. S. Bates, D. E. Discher, and D. A. Hammer, Science **284**, 1143 (1999).
[35]Y. Zhou and R. M. Raphael, Biophys. J. **89**, 1789 (2005).
[36]S. Timoshenko and S. Woinowsky-Krieger, *Theory of Plates and Shells*, Engineering Societies Monographs, 2nd ed. (McGraw-Hill, New York, 1959).
[37]A. Hategan, R. Law, S. Kahn, and D. E. Discher, Biophys. J. **85**, 2746 (2003).
[38]E. A. Evans and R. Skalak, *Mechanics and Thermodynamics of Biomembranes* (CRC, Boca Raton, FL, 1980).
[39]D. Di Carlo, K.-H. Jeong, and L. P. Lee, Lab Chip **3**, 287 (2003).
[40]E. A. Evans, R. Waugh, and L. Melnik, Biophys. J. **16**, 585 (1976).
[41]M. G. Schrlau, N. J. Dun, and H. H. Bau, ACS Nano **3**, 563 (2009).
[42]I. U. Vakarelski, S. C. Brown, K. Higashitani, and B. M. Moudgil, Langmuir **23**, 10893 (2007).